Review

J. Veerabhadra* and Sulake Nagaraja Rao

Comparative assessment of high gain boost converters for renewable energy sources and electrical vehicle applications

Abstract: Due to greenhouse gas emissions and the energy crisis, the conventional way of generation of electricity using fossil fuels is being substituted with Renewable Energy Sources (RES) like solar photovoltaics (SPV), fuel cells, wind, etc. The voltage produced by RES is very small in magnitude; therefore, the choice of DC–DC converter is critical for regulating and improving the output of RES to its maximum level. To meet the power requirement for the utility grid and electric vehicles (EV), the voltage must be enhanced. So far, various types of high-gain DC–DC boost converter (HG-BC) topologies have been suggested. An overview of HG-BC topologies for RES and EV applications is presented in this paper, which provides a unique, extensive, perceptive, and comparative analysis of HG-BC topologies. The mathematical modeling and operating principles of each converter topology have been analyzed and discussed. The boost factor (B) and component count for various HG-BC are thoroughly compared for a 0.5 duty cycle using the MATLAB/Simulink tool.

Keywords: EV; fuel cell; HG-BC and boost factor; RES; SPV; wind.

1 Introduction

The exponential rise in global population results in the rise in energy demand. Because of greenhouse gas emissions, meeting the global energy needs using traditional methods of power generation harms the environment and causes energy shortages (Acar and Dincer 2017; Hossain et al. 2018; Khare et al. 2013; Perera 2018; Reddy 2021; Zhang et al. 2016).

As a result, RES like SPV, fuel cells, and wind are replacing the generation of electricity from fossil fuels (Pranupa, Sriram, and Nagaraja Rao 2022). These RES have been expanding quickly and are expected to triple in the near future (Forouzesh et al. 2017; Manikandan and Vadivel 2013; Mumtaz et al. 2021; Purushothaman et al. 2022; Raghavendra et al. 2019; Shahir et al. 2017). RES presently accounts for 25% of electricity generation capacity across the global. RES is not only efficient, but also beneficial to the environment and low-maintenance. To meet the power requirements for the utility grid and EV, the RES system must integrate a suitable HG-BC to boost and vary the output voltage (V_{out}) (Ali et al. 2014; Forouzesh et al. 2017; Kabalo et al. 2010; Navamani et al. 2022; Raghavendra et al. 2019; Radhika and Margaret 2021; Zaid et al. 2021). The various types of HG–BC are investigated in detail (Ahmad et al. 2018; Aihsan et al. 2022; Dawood 2016; Gore et al. 2019; Hasanpour et al. 2022; Mansour et al. 2022; Raveendhra et al. 2022; Radhika and Margaret 2021; Suryoatmojo et al. 2018; Wu et al. 2015). The RES output voltage is low in magnitude; therefore, the choice of DC–DC converter is critical for varying and improving to get the highest V_{out}.

The transition from traditional, depletable energy sources to renewable, sustainable energy sources necessitates adaptive, high-efficiency power electronic converters and energy infrastructure (Alghaythi et al. 2020; Elsayad et al. 2018; Hossain et al. 2018; Meinagh et al. 2019; Mumtaz et al. 2021; Naresh et al. 2021; Rahimi et al. 2021; Wu et al. 2015; Zaid et al. 2021, 2022). The need for high DC voltage necessitates the use of HG-BC. The HG-BC is employed in a wide range of industries, including solar PV, robotics, aerospace, medical equipment, high voltage DC systems, and EVs (Jagadeesh and Indragandhi 2022; Mansour and Zaky 2023; Matam et al. 2018; Navamani et al. 2022; Rehman et al. 2015; Samuel et al. 2020; Sivakumar et al. 2016).

A typical RES incorporated with HG-BC is depicted in Figure 1. The voltage of the SPV and fuel cell is DC, and they are coupled directly to a low-voltage DC bus. The output of a wind turbine is AC, which must be converted into DC and then given to a low-voltage DC bus. The RES system V_{out} is low, and it is required to be converted into high-voltage DC
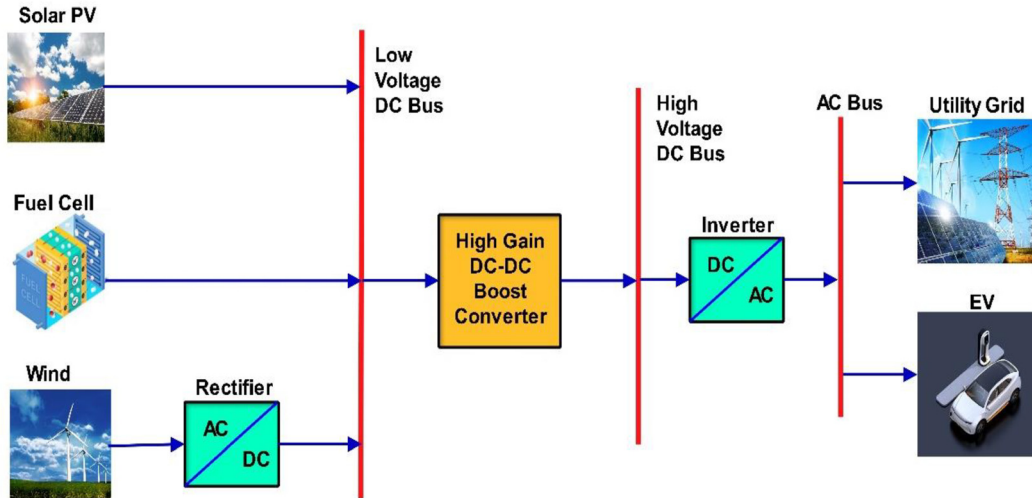
*Corresponding author: J. Veerabhadra, Department of Electrical Engineering, M S Ramaiah University of Applied Sciences, Bangalore, India, E-mail: veerabhadra.ee.et@msruas.ac.in
Sulake Nagaraja Rao, Department of Electrical Engineering, M S Ramaiah University of Applied Sciences, Bangalore, India

Figure 1: A typical RES integrated with HG-BC.

for utility grid and EV applications. Therefore, the use of HG-BC is essential.

The types of HG-BC for RES and EV applications are depicted in Figure 2. The major focus of this research is on non-isolated HG-BC. The use of passive elements and semiconductor devices, together with regulating the duty cycle of the control circuit, results in a high gain (Dawood 2016; Nagaraja Rao et al. 2022; Radhika and Margaret 2021; Rahimi et al. 2021; Raveendhra et al. 2022; Wu et al. 2015).

In comparison to the input voltage, the voltage in BC is higher (Varanasi, Nagaraja Rao, and Duraiswamy 2023). For a buck-boost converter, the polarity of the converter voltage is inverted, and the magnitude of the V_{out} is increased or decreased. The Cuk converter's output is also inverted, producing voltages of greater or lesser magnitude. The Cuk and Buck-Boost converters' gain remains constant (Chandrasekar et al. 2020). The SEPIC converter can be used to raise or lower the V_{out} without reversing the output polarity (Moradpour et al. 2017; Maroti et al. 2019; Sabzali et al. 2015). The Z-Source converter is an efficient converter. The features of this converter is to step up and down the V_{out} (Rao, Veerabhadra, and Kumar 2020; Torkan and Ehsani 2018). The topology of the Zeta converter is also called the power optimizer. The features of this converter are constant output current, non-inverting
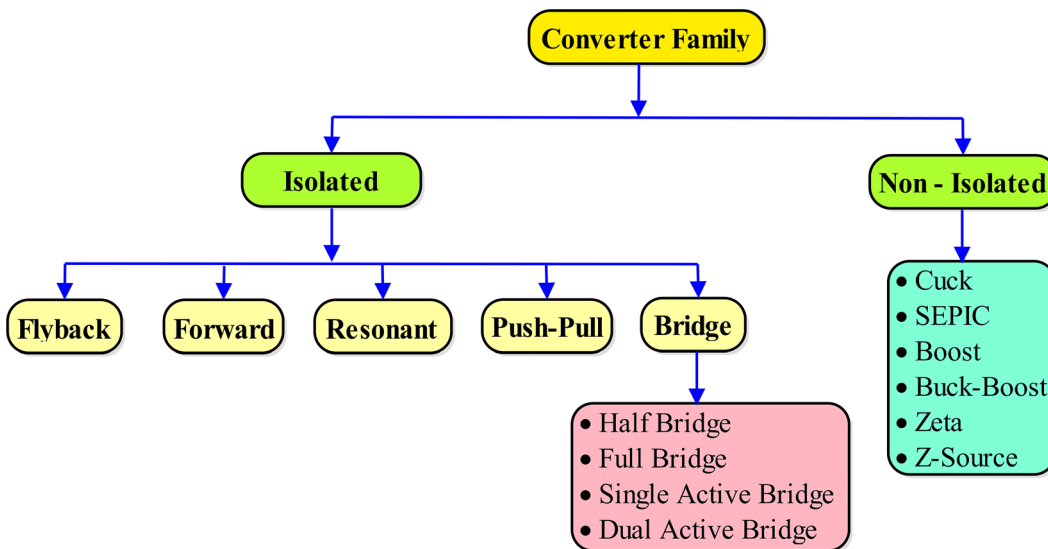

Figure 2: Classifications of DC–DC converter for RES and EV applications.

operation, and controlled output voltage. The ripple content in the V_{out} is low (Hosseini et al. 2015; Keerthana and Chintu 2017).

The conventional BC is shown in Figure 3. The output is too low for utility grid supply, and the boost factor is adjusted to 2. One of the main drawbacks of traditional BC is its low value of B.

The gain of conventional BC is given by

$$\frac{V_{out}}{V_{PV}} = \frac{1}{(1-D)} \tag{1}$$

For a 0.5 duty cycle, the value of B equals 2. With the use of HG-BC, the limitations of conventional BC can be overcome.

In this paper, the following HG-BC are discussed in detail in terms of operation, mathematical modeling, and comparison, with component count and boost factor (B):

  i. Conventional Boost Converter (BC)
 ii. High Gain Quadratic Following Boost Converter(HG-QFBC)
iii. High Gain Quadratic Boost converter (HG-QBC)
iv. High Gain Interleaved Boost Converter (HG-IBC)
 v. High Gain Improved Quadratic Boost Converter (HG-IQBC)
vi. High Gain Cubic Boost Converter (HG-CBC)

Furthermore, simulation of the aforementioned HG-BC topologies has been performed using the MATLAB/Simulink tool. The primary goal of this research is to afford a detailed, perceptive, and comparative analysis of HG-BC topologies.

2 Mode of operation and mathematical analysis of HG-QFBC topology

2.1 Operation of HG-QFBC topology

The suggested HG-QFBC is depicted in Figure 4. It comprises of two semiconductor switches (S_1 and S_2), three diodes
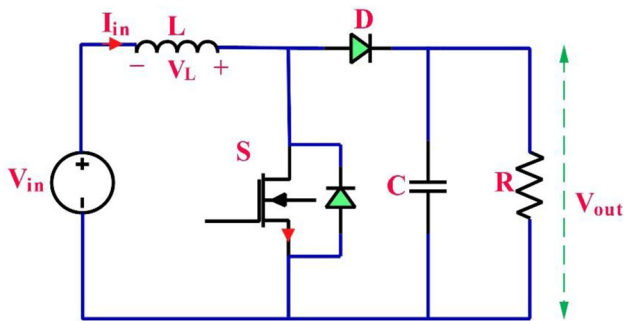

Figure 3: Conventional boost converter.

(D_1, D_2 and D_3), three capacitors (C_1, C_2 and C_3), two inductors (L_1 and L_2), and at last resistive load (R). The HG-QFBC uses a two switches (S_1 and S_2) to regulate the V_{out}.

2.2 Mode of operation – I

The operating mode-1 of HG-QFBC is represented in Figure 5. It comprises of two semiconducting switches (S_1 and S_2) that will be turned on constantly. An open circuit will be formed by the two diodes (D_1 and D_3). The diode (D_2) will be in conduction. The input source charges the L_1, the inductor (L_2) is excited by the capacitors' (C_1 and C_2) voltage, and the capacitor (C_3) delivers current to the resistive load (R).

The voltage of (L_1 and L_2) is derived by applying KVL to Figure 5.

$$V_{L1} = V_{in} \tag{2}$$

$$V_{L2} = V_{C1} \tag{3}$$

2.3 Mode of operation – II

The mode of operation II for HG-QFBC is represented in Figure 6. The two semiconducting switches (S_1 and S_2) will be switched off. The first two diodes (D_1 and D_3) will be in conduction mode, while the third (D_2) will become open. L_1 and L_2 will demagnetize and charge C_1, C_2, and C_3.

The voltage of (L_1 and L_2) is obtained by using KVL to Figure 6.

$$V_{L1} = V_{in} + V_{C1} \tag{4}$$

$$V_{L2} = V_{out} - V_{C1} - V_{C2} - V_{in} \tag{5}$$

2.4 Mathematical analysis

The voltage of each inductors (L_1 and L_2) is determined using volt-sec balance.

The voltage of L_1 is obtained as

$$\int_0^T V_{L1}(t)dt = 0 \tag{6}$$

$$\int_0^{DT} V_{C1}dt + \int_{DT}^T (V_{in} + V_{C1})dt = 0 \tag{7}$$

$$V_{in}[t]_0^{DT} + (V_{in} + V_{C1})[t]_{DT}^T = 0 \tag{8}$$

$$V_{in}(DT) + (V_{in} + V_{C1})(1-D)T = 0 \tag{9}$$
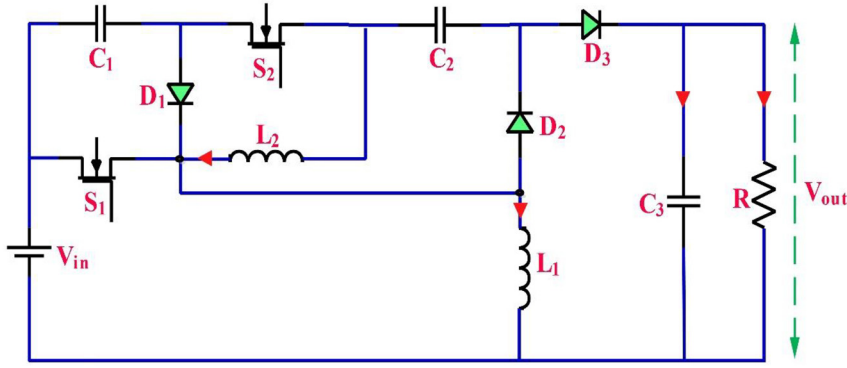
The voltage of C_1 is obtained as

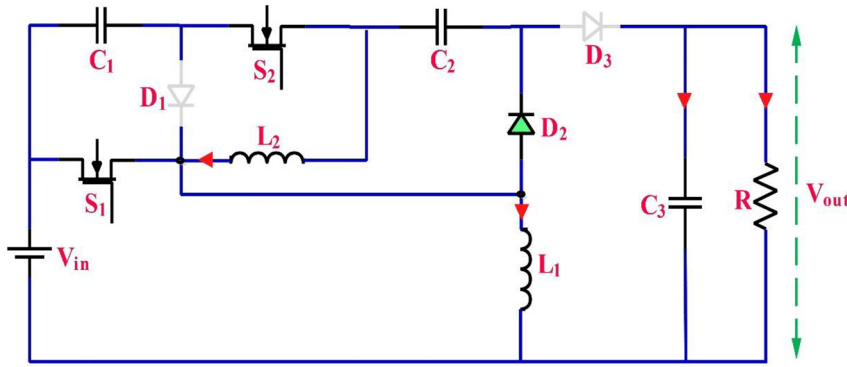**Figure 4:** HG-QFBC connected to RES.

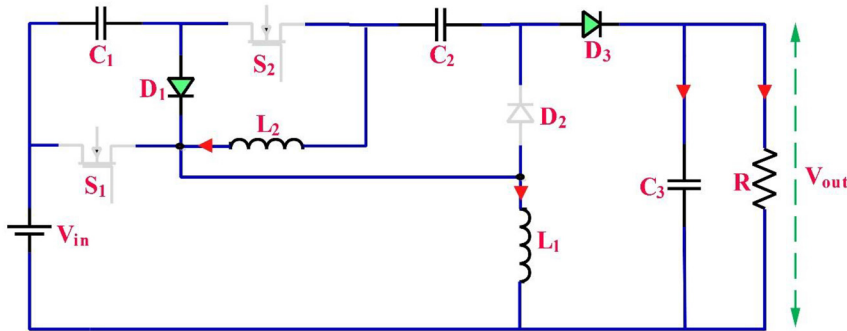**Figure 5:** Mode of operation-I of HG-QFBC.

Figure 6: Mode – II operation of HG-QFBC.

$$V_{in} = -V_{C1}(1-D) \tag{10}$$

$$V_{C1} = -\frac{V_{in}}{(1-D)} \tag{11}$$

The voltage across L_2 is given by

$$\int_0^T V_{L2}(t)dt = 0 \tag{12}$$

$$\int_0^{DT}(V_{C1}+V_{in})dt + \int_{DT}^T (V_{out}-V_{C1}-V_{C2}-V_{in})dt = 0 \tag{13}$$

$$(V_{C1}+V_{in})[t]_0^{DT} + (V_{out}-V_{C1}-V_{C2}-V_{in})[t]_{DT}^T = 0 \tag{14}$$

The voltage of C_2 is obtained as

$$V_{C2}(1-D) = V_{in} \tag{15}$$

$$V_{C2} = \frac{V_{in}}{(1-D)} \tag{16}$$

The gain (G) of the HG-IQBC is given as

$$\frac{V_{out}}{V_{in}} = \frac{(1-D+D^2)}{(1-D)^2} \tag{17}$$

The equation (17) represents, G of the HG-QFBC. For 0.5 duty cycle (D), the value of B is 3.

3 Mode of operation and mathematical analysis of HG-QBC topology

3.1 Operation of HG-QBC topology

The topology of HG-QBC is shown in Figure 7. It comprises a switch (S), three diodes (D_1, D_2, and D_3), two capacitors (C_1 and C_2), two inductors (L_1 and L_2), and at last a resistive load (R). The HG-QBC uses only one switch (S) to regulate the V_{out}.

3.2 Mode of operation-I

The operating mode I of HG-QBC is represented in Figure 8. The switch (S) is switched on, and the diode (D_1) will conduct. The diodes (D_2 and D_3) will form an open circuit. The voltage from the input source will charge the inductor (L_1) and capacitor (C_1). The charged capacitor (C_2) helps deliver current to the resistive load (R).

The voltages of (L_1, and L_2) is derived by applying KVL to Figure 8.

$$V_{L1} = V_{in} \tag{18}$$

$$V_{L2} = V_{C1} \tag{19}$$

3.3 Mode of operation – II

The mode of operation II for HG-QBC is represented in Figure 9. The switch (S) is switched off. The diode (D_1) will be open, and the other two diodes (D_2 and D_3) are in conduction mode. The inductors (L_1 and L_2) will be de-energized, and the capacitors (C_1 and C_2) will get charged.

The voltage of (L_1 and L_2) is derived by applying KVL to Figure 9.

$$V_{L1} = V_{in} - V_{C1} \tag{20}$$

$$V_{L2} = V_{C1} - V_{C2} \tag{21}$$

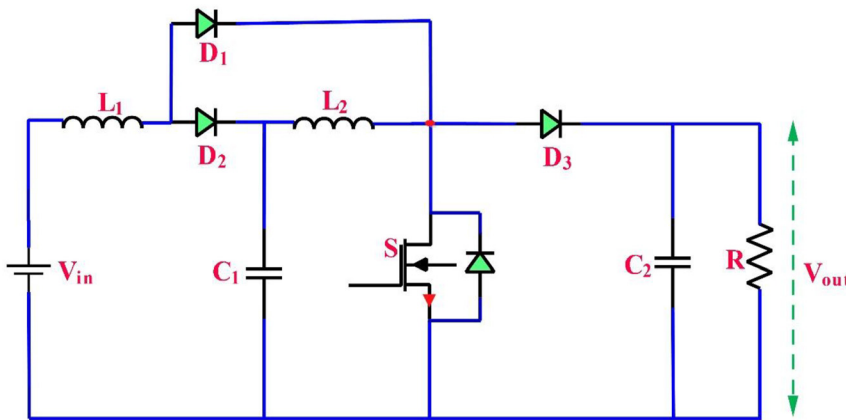$$V_{L2} = V_{C1} - V_{out} \tag{22}$$
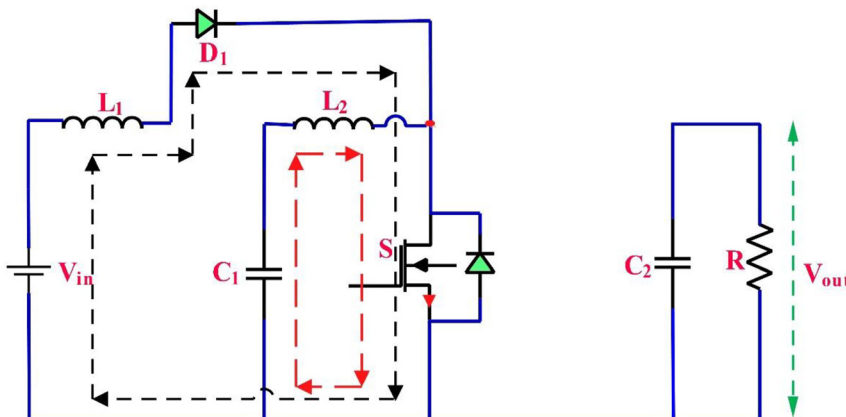

Figure 7: HG-QBC connected to RES.
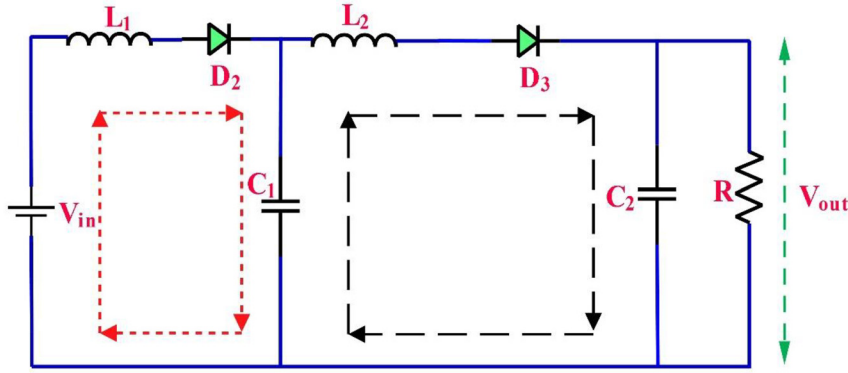

Figure 8: Mode-I operation of HG-QBC.

Figure 9: Mode of operation-II for HG-QBC.

3.4 Mathematical analysis

By using the volt-sec balance, the voltages of (L_1, and L_2) is determined.

The voltage across L_1

$$\int_0^T V_{L1}(t)dt = 0 \tag{23}$$

$$\int_0^{DT} V_{in}dt + \int_{DT}^T (V_{PV} - V_{C1})dt = 0 \tag{24}$$

$$V_{in}[t]_0^{DT} + (V_{in} - V_{C1})[t]_{DT}^T = 0 \tag{25}$$

The capacitor (C_1) voltage is obtained as

$$V_{in} = V_{C1}(1 - D) \tag{26}$$

$$V_{C1} = \frac{V_{in}}{(1 - D)} \tag{27}$$

The voltage across L_2 is obtained as

$$\int_0^T V_{L2}(t)dt = 0 \tag{28}$$

$$\int_0^{DT} V_{C1}dt + \int_{DT}^T (V_{C1} - V_{out})dt = 0 \tag{29}$$

$$V_{C1}[t]_0^{DT} + (V_{C1} - V_{out})[t]_{DT}^T = 0 \tag{30}$$

The capacitor (C_2) voltage is given as

$$V_{C2} = V_{out}(1 - D) \tag{31}$$

$$V_{out} = \frac{V_{C1}}{(1 - D)} = \frac{V_{PV}}{(1 - D)^2} \tag{32}$$

The G of HG-QBC is obtained as

$$\frac{V_{out}}{V_{in}} = \frac{1}{(1 - D)^2} \tag{33}$$

The G of HG-QBC is represented by equation (33). The boost factor is 4 for a 0.5 D.

4 Mode of operation and mathematical analysis of HG-IBC topology

4.1 Operation of HG-IBC topology

The suggested HG-IBC is represented in Figure 10. It contains three semiconducting switches (S_1, S_2, and S_3), three diodes (D_1, D_2, and D_3), three capacitors (C_1, C_2, and C_3), three inductors (L_1, L_2, and L_3), and at last a resistive load (R). The suggested HG-IBC uses three switches (S_1, S_2, and S_3) to control the V_{out}.

4.2 Mode of operation-I

The operating mode I of HG-IBC is represented in Figure 11. It contains three semiconducting switches (S_1, S_2, and S_3) that will be switched on simultaneously. The three diodes (D_1, D_2, and D_3) will become an open circuit. The input source energizes the L_1, L_2, and L_3. C_1 is disconnected from the input supply and the loading. The voltages of the capacitors (C_2 and C_3) delivers the current to the resistive load (R).

4.3 Mode of operation-II

The mode of operation II for HG-IBC is represented in Figure 12. The switches (S_1 and S_3) will be deactivated by being turned off, and the switch (S_2) will be on. The two diodes (D_1 and D_3) will be in conduction, and the third diode (D_2) will be turned off due to an open circuit. The two capacitors (C_1 and C_3) will get charged from the input source. The voltage supplied by the capacitor (C_2) delivers the current to the resistive load (R).
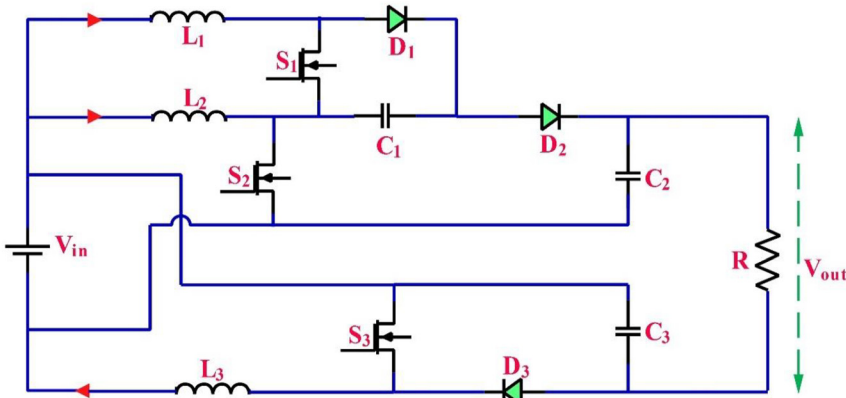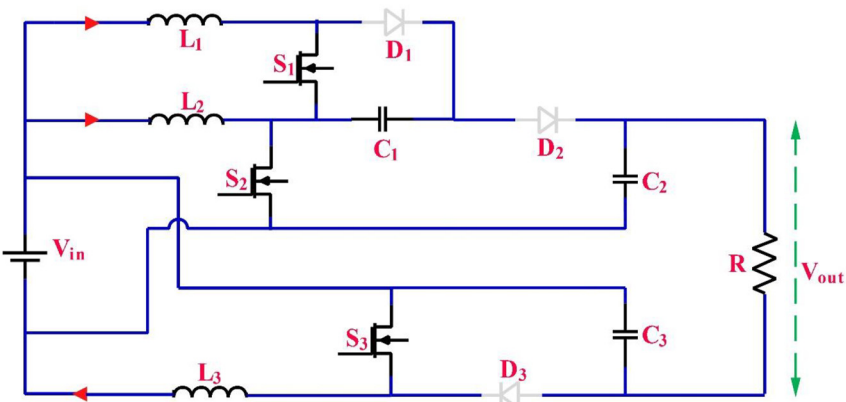
Figure 10: HG-IBC connected to RES.

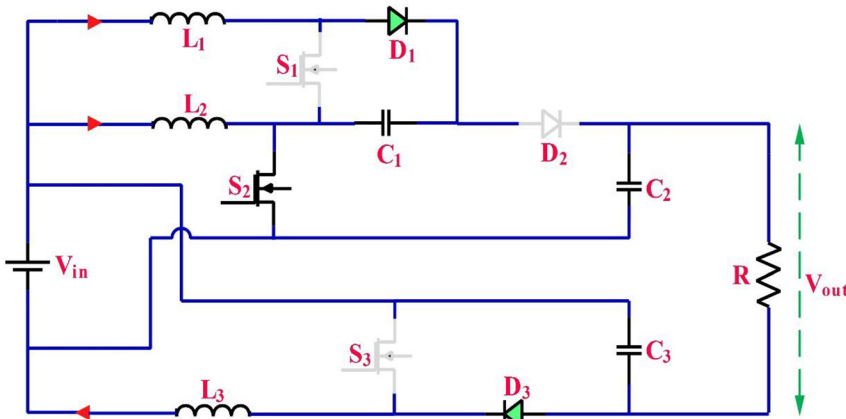**Figure 11:** Mode of operation-I for HG-IBC.

Figure 12: Mode of operation-II for of HG-IBC.

4.4 Mode of operation-III

The operating mode III of the HG-IBC is represented in Figure 13. This operating mode is just the reverse of mode II operation. The switches (S_1 and S_3) will be on and the other switch (S_2) will be switched off. The two diodes (D_1 and D_3) will be turned off due to the open circuit, and the third diode (D_2) will be in conduction. The capacitor (C_2) will get charged

from the input source. The two capacitors (C_1 and C_3) deliver the current to the resistive load (R).

4.5 Mathematical analysis

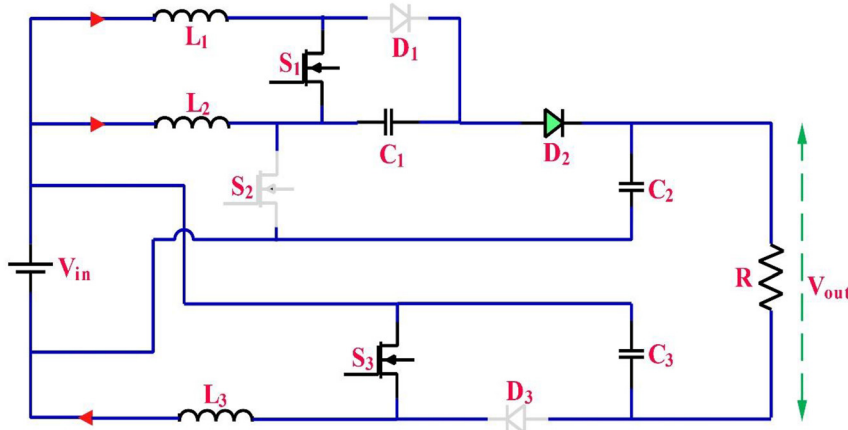The voltages of L_1, L_2 and L_3 is determined using volt-sec balance.

Figure 13: Mode of operation-III for HG-IBC.

The voltage of L_1 is given as

$$V_{L1} = V_{in}(t_1 - t_2) + (V_{in} - V_{C1})(t_2 - t_1) + V_{in}(t_3 - t_2)$$
$$+ V_{in}(t_4 - t_3)$$
$$= 0 \tag{34}$$

The capacitor (C_1) voltage is obtained as

$$V_{C1} = \frac{V_{in}}{1 - D} \tag{35}$$

The voltage of L_2 is obtained as

$$V_{L2} = V_{in}(t_1 - t_0) + V_{in}(t_2 - t_1) + V_{in}(t_3 - t_2)$$
$$+ (V_{in} + V_{C1} - V_{C2})(t_4 - t_3)$$
$$= 0 \tag{36}$$

The capacitor (C_2) voltage is given as

$$V_{C2} = \frac{V_{in}}{1 - D} + V_{C1} \tag{37}$$

By substituting the above equation (35) in (37), we get

$$V_{C2} = \frac{V_{in}}{1 - D} + \frac{V_{in}}{1 - D}$$

$$V_{C2} = \frac{2\,V_{in}}{1 - D} \tag{38}$$

The voltage of L_3 is obtained as

$$V_{L3} = V_{in}(t_1 - t_0) + (V_{in} - V_{C3})(t_2 - t_1) + V_{in}(t_3 - t_2)$$
$$+ V_{in}(t_4 - t_3)$$
$$= 0 \tag{39}$$

The capacitor (C_3) voltage is given as

$$V_{C3} = \frac{V_{in}}{1 - D} \tag{40}$$

The voltage output of HG-IBC is given as

$$V_0 = V_{C2} + V_{C3} - V_{in} \tag{41}$$

$$V_0 = \frac{2\,V_{in}}{1 - D} + \frac{V_{in}}{1 - D} - V_{in} \tag{42}$$

The G of the HG-IBC is given as

$$\frac{V_0}{V_{in}} = \frac{2 + D}{1 - D} \tag{43}$$

The G of HG-IBC is represented in equation (43). The value of boost factor is 5 for 0.5 D.

5 Mode of operation and mathematical analysis of HG-IQBC topology

5.1 Operation of HG-IQBC topology

The suggested HG-IQBC is depicted in Figure 14. It contains two semiconductor switches (S_1 and S_2), three diodes (D_1, D_2, and D_3), three capacitors (C_1, C_2, and C_3), two inductors (L_1 and L_2), and, at last, the resistive load (R). The HG-IQBC converter uses two switches (S_1 and S_2) to regulate the V_{out}.

5.2 Mode-I operation

The HG-IQBC for mode I of operation is represented in Figure 15. It consists of two semiconducting switches (S_1 and S_2) that will be switched on constantly. The three diodes (D_1, D_2, and D_3) will be switched off and become an open circuit. The inductor (L_1) will get charged from the input source, the voltage supplied by two capacitors (C_1 and C_2) will energize the L_2, and the voltage across C_3 will deliver the current to the resistive load (R).
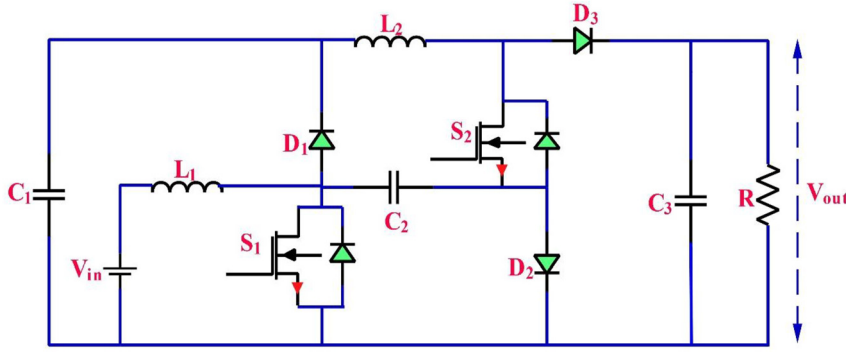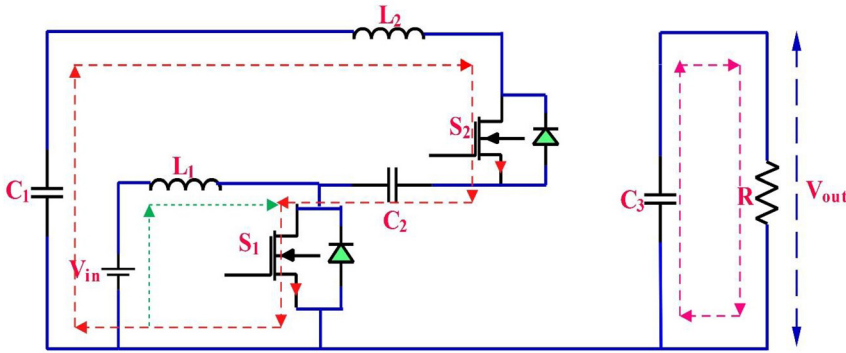
Figure 14: HG-IQBC connected to RES.

Figure 15: Mode-I operation of HG-IQBC.

The voltage of (L_1 and L_2) is derived by applying KVL to Figure 15.

$$V_{L1} = V_{in} \tag{44}$$

$$V_{L2} = V_{C1} + V_{in} = V_{C2} + V_{in} \tag{45}$$

5.3 Mode of operation-II

The suggested mode of operation II for HG-IQBC is represented in Figure 16. The two semiconducting switches (S_1 and S_2) will be off. The three diodes (D_1, D_2, and D_3) will be in conduction. The inductors (L_1 and L_2) will be de-energized, and the capacitors (C_1, C_2, and C_3) will get charged.

The inductors (L_1 and L_2) voltage is derived by applying KVL to Figure 16.

$$V_{L1} = V_{in} - V_{C1} = V_{in} - V_{C2} \tag{46}$$

$$V_{L2} = V_{C1} - V_{out} \tag{47}$$

5.4 Mathematical analysis

The voltage of Inductors (L_1 and L_2) is used to determine by applying volt-sec balance.

The voltage across L_1 is obtained as

$$\int_0^T V_{L1}(t)dt = 0 \tag{48}$$

$$\int_0^{DT} V_{in}dt + \int_{DT}^T (V_{in} - V_{C1})dt = 0 \tag{49}$$

$$V_{in}[t]_0^{DT} + (V_{in} - V_{C1})[t]_{DT}^T = 0 \tag{50}$$

The capacitor (C_1 and C_2) voltage is given as

$$V_{in} = V_{C1}(1 - D) \tag{51}$$

$$V_{C1} = V_{C2} = \frac{V_{in}}{(1 - D)} \tag{52}$$

The voltage of L_2 is given by

$$\int_0^T V_{L2}(t)dt = 0 \tag{53}$$

$$\int_0^{DT} (V_{C1} + V_{in})dt + \int_{DT}^T (V_{C1} - V_{out})dt = 0 \tag{54}$$

$$(V_{C1} + V_{in})[t]_0^{DT} + (V_{C1} - V_{out})[t]_{DT}^T = 0 \tag{55}$$

The capacitor (C_3) voltage is given as

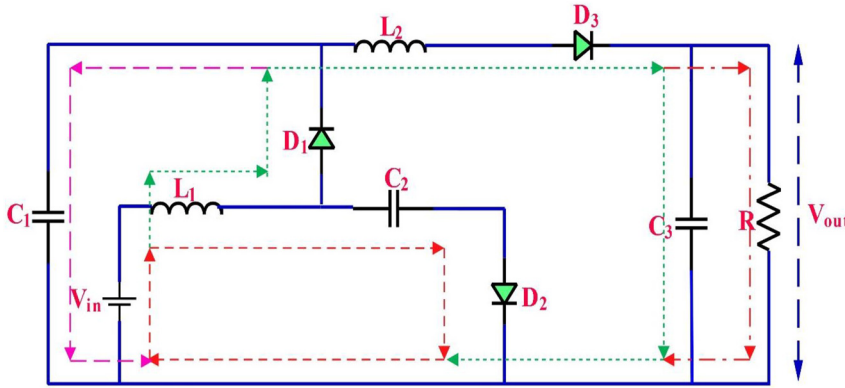$$V_{C1}(1 + D) = V_{out}(1 - D) \tag{56}$$

Figure 16: Mode of operation-II for HG-IQBC.

$$V_{out} = \frac{V_{C1}(1+D)}{(1-D)} = \frac{V_{in}(1+D)}{(1-D)^2} \qquad (57)$$

The gain of the HG-IQBC is obtained as

$$\frac{V_{out}}{V_{in}} = \frac{(1+D)}{(1-D)^2} \qquad (58)$$

The equation (58) represents the gain of HG-IQBC. The boost factor is 6 for 0.5 duty cycle (D).

6 Mode of operation and mathematical analysis of HG-CBC topology

6.1 Operation of HG-CBC topology

The suggested HG-CBC is shown in Figure 17. It contains one semiconducting switch (S), three inductors (L_1, L_2, and L_3), three capacitors (C_1, C_2, and C_3), five diodes ($D_1, D_2, D_3, D_4,$ and D_5), and a resistive load (R). The HG-CBC uses only one switch (S) to regulate the V_{out}, and it has two modes of operation.

6.2 Mode of operation-I

The operating mode I of HG-CBC is represented in Figure 18. The semiconducting switch (S) is switched on. The two diodes (D_1 and D_3) will be in conduction mode, and the other three diodes ($D_2, D_4,$ and D_5) will act in open circuit. The input source will charge the inductor (L_1), the inductor (L_2) will get excited from the capacitor (C_1) voltage, and finally the inductor (L_3) will be excited from the capacitor (C_2) voltage. The voltage of capacitor (C_3) delivers the current to the resistive load (R).

The inductors (L_1, L_2 and L_3) voltage is derived by applying KVL to Figure 18.

$$V_{L1} = V_{PV} \qquad (59)$$

$$V_{L2} = V_{C1} \qquad (60)$$

$$V_{L3} = V_{C2} \qquad (61)$$

6.3 Mode of operation-II

The circuit diagram in Figure 19 shows the mode of operation II of the HG-CBC. The switch (S) will be switched off. The two diodes (D_1 and D_3) will function as an open circuit, and the other three diodes ($D_2, D_4,$ and D_5) will be under conduction. The inductors (L_1, L_2, and L_3) will be de-energized, and the capacitors (C_1, C_2, and C_3) will get charged.

The voltages of (L_1, L_2 and L_3) is derived by applying KVL to Figure 19.

$$V_{L1} = V_{PV} - V_{C1} \qquad (62)$$

$$V_{L2} = V_{C1} - V_{C2} \qquad (63)$$

$$V_{L3} = V_{C2} - V_{out} \qquad (64)$$

6.4 Mathematical analysis

By employing volt-sec balance, the voltage of L_1, L_2 and L_3 is obtained.

The voltage L_1 is obtained as

$$\int_0^T V_{L1}(t)dt = 0 \qquad (65)$$

$$\int_0^{DT} V_{PV}dt + \int_{DT}^T (V_{PV} - V_{C1})dt = 0 \qquad (66)$$

$$V_{PV}[t]_0^{DT} + (V_{PV} - V_{C1})[t]_{DT}^T = 0 \qquad (67)$$

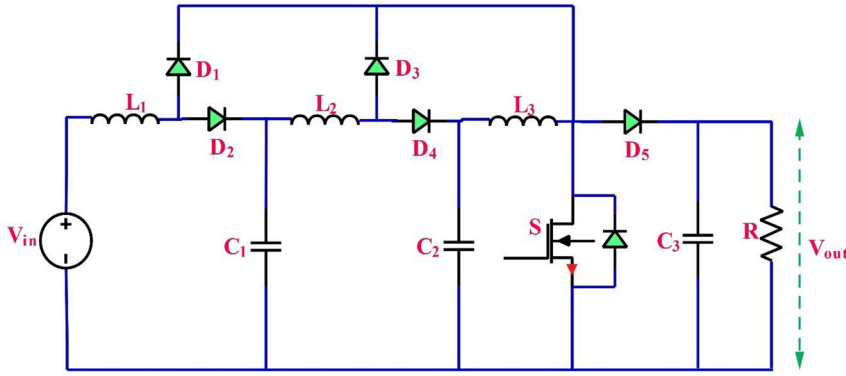The capacitor (C_1) voltage is given as
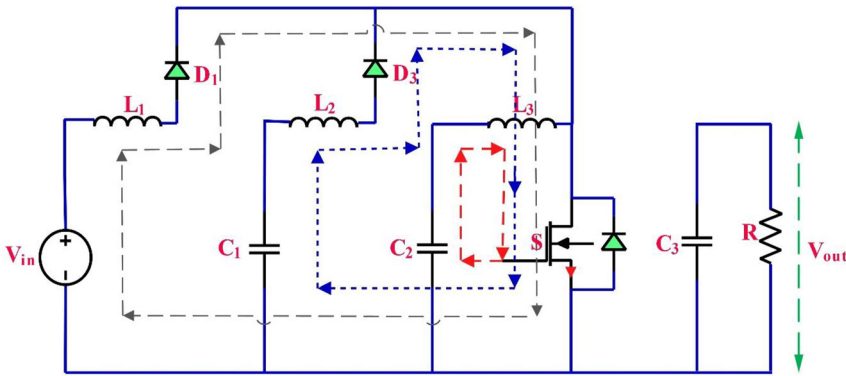
Figure 17: HG-CBC connected to RES.

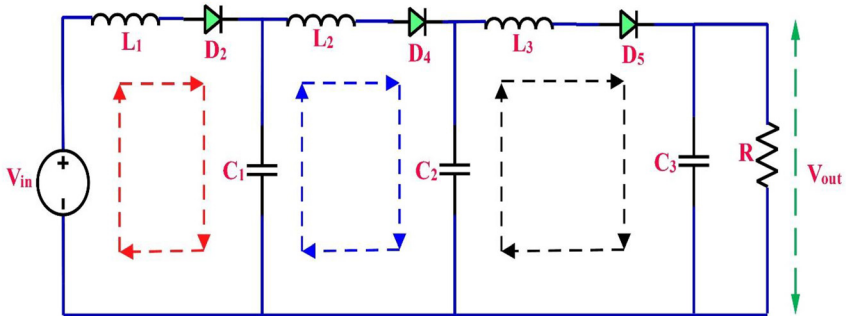**Figure 18:** Mode-I operation of HG-CBC.

Figure 19: Mode of operation-II for HG-CBC.

$$V_{PV} = V_{C1}(1 - D) \tag{68}$$

$$V_{C1} = \frac{V_{PV}}{(1 - D)} \tag{69}$$

The voltage of inductor (L_2) is obtained as

$$\int_0^T V_{L2}(t)dt = 0 \tag{70}$$

$$\int_0^{DT} V_{C1}dt + \int_{DT}^T (V_{C1} - V_{C2})dt = 0 \tag{71}$$

$$V_{C1}[t]_0^{DT} + (V_{C1} - V_{C2})[t]_{DT}^T = 0 \tag{72}$$

The capacitor (C_2) voltage is given as

$$V_{C1} = V_{C2}(1 - D) \tag{73}$$

$$V_{C2} = \frac{V_{C1}}{(1 - D)} = \frac{V_{PV}}{(1 - D)^2} \tag{74}$$

The voltage of inductor (L_3) is obtained as

$$\int_0^T V_{L3}(t)dt = 0 \tag{75}$$

$$\int_0^{DT} V_{C2}dt + \int_{DT}^T (V_{C2} - V_{out})dt = 0 \tag{76}$$

$$V_{C2}[t]_0^{DT} + (V_{C2} - V_{out})[t]_{DT}^T = 0 \tag{77}$$

The voltage of capacitor C_3 is given by

$$V_{C2} = V_{out}(1 - D) \tag{78}$$

$$V_{out} = V_{C3} = \frac{V_{C2}}{(1-D)} = \frac{V_{PV}}{(1-D)^3} \tag{79}$$

$$\frac{V_{out}}{V_{PV}} = \frac{1}{(1-D)^3} \tag{80}$$

The gain of HG-CBC is represented in equation (80). The boost factor is 8 for 0.5 duty cycle.

7 Comparative analysis of boost factor for various HG-BC

Figure 20 shows the boost factors for different HG-BC with different duty cycles. For a 0.5 duty cycle, the boost factor (B) for a conventional boost converter is 2. For HG-QFBC, B is equal to 3. The value of B is equal to 4 for HG-QBC. The value of B for HG-IBC is 5. The value of B for HG-IQBC is 6. B for HG-CBC is equal to 8. In comparison with all HG-BC, the highest boost factor for HG-CBC is 8 for 0.5 duty cycle.

Based on component counts and boost factors for 0.5 duty cycle, Table 1 compares various HG-BCs in detail.

Table 2 shows a comparative analysis of various boost converter configurations with specifications and features.

8 Results and discussion

Figure 21 shows the RES voltage output and HG-QFBC. RES's V_{out} is 25 V, which is very low. It must be improved for grid-connected operation. The conventional BC output is twice the value of the boost factor, resulting in a V_{out} of 50 V.

**Table 1:** Component count and boost factor comparison of various HG-BC.

Converter type	Voltage gain	Components					B
		S	D	L	C	Total	
Conventional BC	$\frac{1}{1-D}$	1	1	1	1	4	2
HG-QFBC (Veerachary and Kumar 2020)	$\frac{(1-D+D^2)}{(1-D)^2}$	2	3	2	3	10	3
HG-QBC (Veerabhadra and Nagaraja Rao 2022)	$\frac{1}{(1-D)^2}$	1	3	2	2	8	4
HG-IBC (Kumar et al. 2022)	$\frac{2+D}{1-D}$	3	3	3	3	12	5
HG-IQBC (Naresh et al. 2021)	$\frac{1+D}{(1-D)^2}$	2	3	2	3	10	6
HG-CBC (Ahmad et al. 2020)	$\frac{1}{(1-D)^3}$	1	5	3	3	12	8

Switches (S), Diodes (D), Inductance (L), Capacitance (C) and Boost factor (B).

This voltage is insufficient for grid integration. As a result, the X HG-QFBC topology is proposed to improve the output by x three times the boost factor, resulting in a total V_{out} of 75 V.
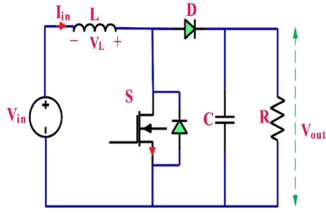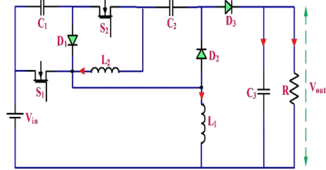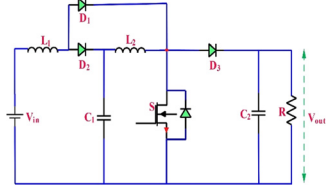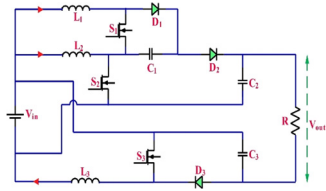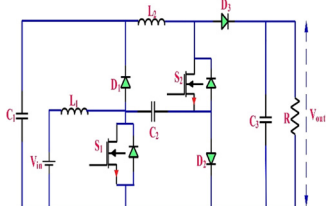
The voltage output of RES and HG-QBC is represented in Figure 22. RES's V_{out} is 25 V, which is very low. It must be improved for grid-connected operation. The V_{out} of conventional BC is twice the value of the boost factor, resulting in a total V_{out} of 50 V. This voltage is insufficient for grid integration. So, the HG-QBC topology is suggested to increase the output by four times, resulting in a V_{out} of 100 V.

The V_{out} of RES and HG-IBC is depicted in Figure 23. RES's V_{out} is 25 V, which is less. It must be improved for grid-connected operation. The V_{out} of conventional BC is two times the boost factor, resulting in a V_{out} of 50 V. This voltage is inadequate for grid integration. So, the HG-IBC topology is suggested to increase the output by five times, resulting in a V_{out} of 125 V.
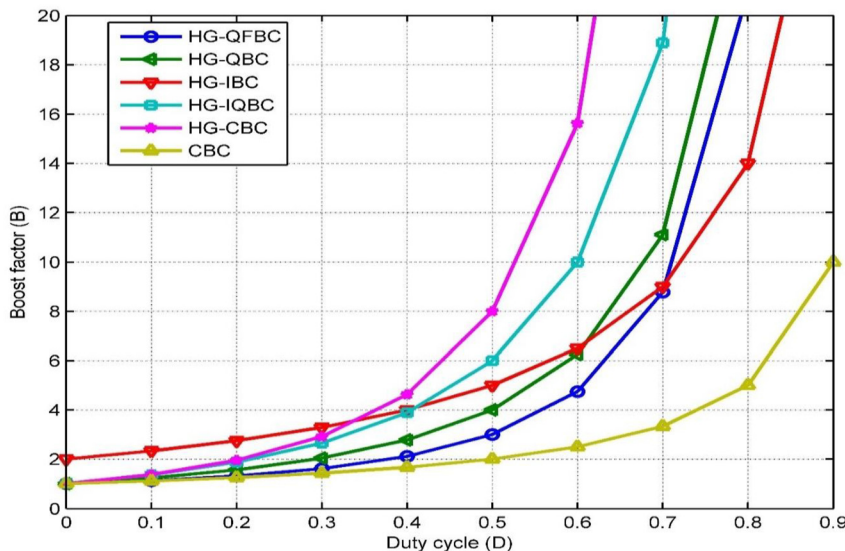
Figure 20: Boost factors of various HG-BC.

Table 2: A comparative analysis of various HG-BC configurations with the features.

Sl. No.	Type of converter	Configuration	Specifications	Features
1.	Conventional BC		L = 160 mH C = 220 μF R = 100 Ω Fs = 50 kHz	The voltage gain of conventional BC is two
2.	HG-QFBC (Veerachary and Kumar 2020)		L_1 = 1600 μH L_2 = 800 μH $C_1 = C_2$ = 47 μF C_3 = 100 μF R = 300 Ω Fs = 100 kHz	Enhances the voltage gain and efficiency
3.	HG-QBC (Veerabhadra and Nagaraja Rao 2022)		L_1 = 0.2 mH L_2 = 0.5 mH C_1 = 9 mF C_2 = 2 mF R = 100 Ω Fs = 100 kHz	Voltage stress is significantly reduced on the switch, diodes, and capacitors.
4.	HG-IBC (Kumar et al. 2022)		L_1 = 0.2 mH L_2 = 0.3 mH L_3 = 5 mH C_1 = 9 μF C_2 = 2 μF C_3 = 1 μF R = 100 Ω Fs = 50 kHz	Obtains smooth output waveforms with less current and voltage ripples and current ripples
5.	HG-IQBC (Naresh et al. 2021)		L_1 = 0.5 mH L_2 = 1 mH $C_1 = C_2$= 24 μF C_3 = 20 μF R = 100 Ω Fs = 50 kHz	The voltage gain of an HG-IQBC is six. High boosting with suppression of inrush current
6.	HG-CBC (Ahmad et al. 2020; Revathi and Prabhakar 2016)		L_1 = 0.2 mH L_2 = 0.3 mH L_3 = 1 mH C_1 = 9 mF C_2 = 2 mF C_3 = 1 mF R = 100 Ω Fs = 100 kHz	High voltage gain with reduced switch stress

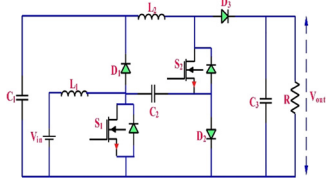The voltage output of RES and HG-IQBC is shown in Figure 24. RES's V_{out} is 25 V, which is very low. It must be improved for grid-connected modes of operation. The conventional BC output is two times the boost factor, resulting in a total V_{out} of 50 V. This voltage is insufficient for grid integration. So, the HG-IQBC topology is proposed to improve the output by six times, resulting in a V_{out} of 150 V.

Figure 25 depicts the voltage output of the RES and HG-CBC. RES's V_{out} is 25 V, which is less. It must be improved for grid-connected modes of operation. The conventional BC
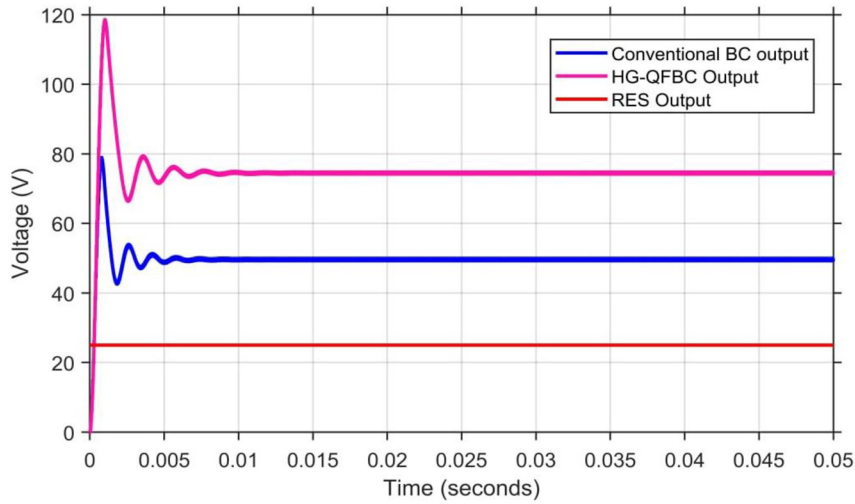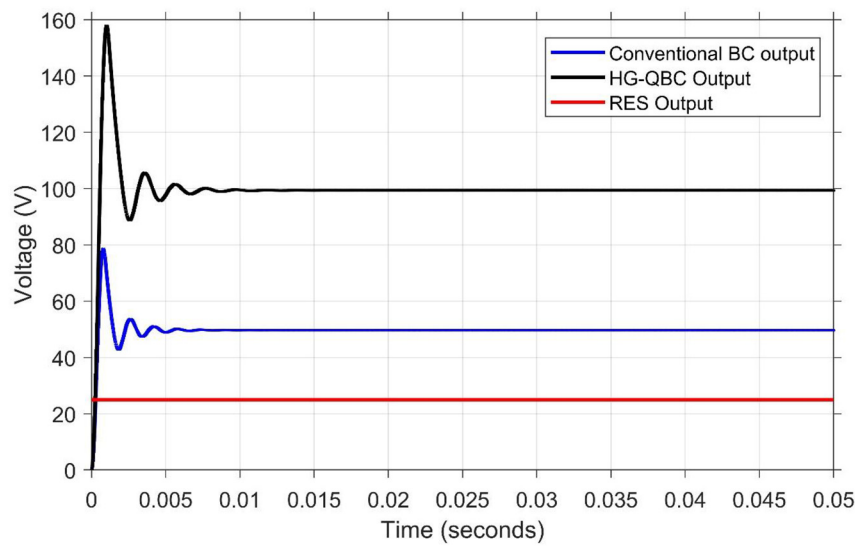
Figure 21: Output voltage of RES and HG-QFBC.

Figure 22: Output voltage of RES and HG-QBC.
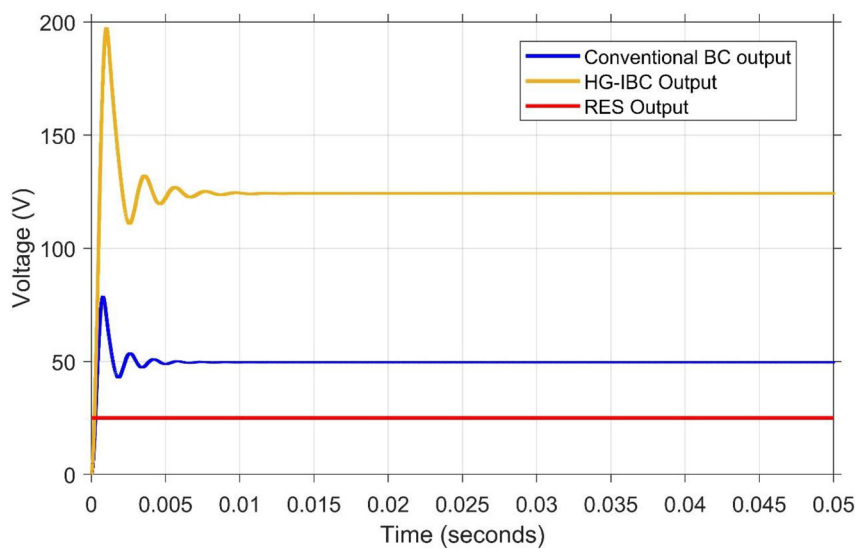
Figure 23: Output voltage of RES and HG-IBC.
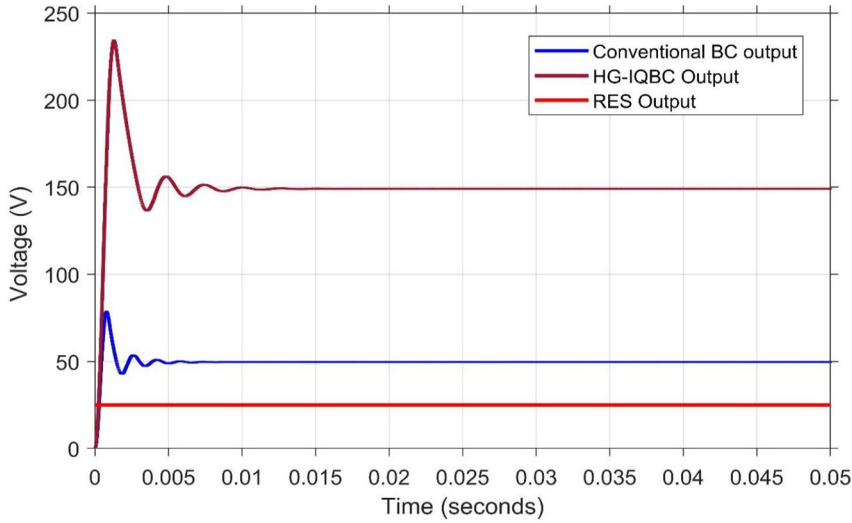
Figure 24: Output voltage of RES and HG-IQBC.
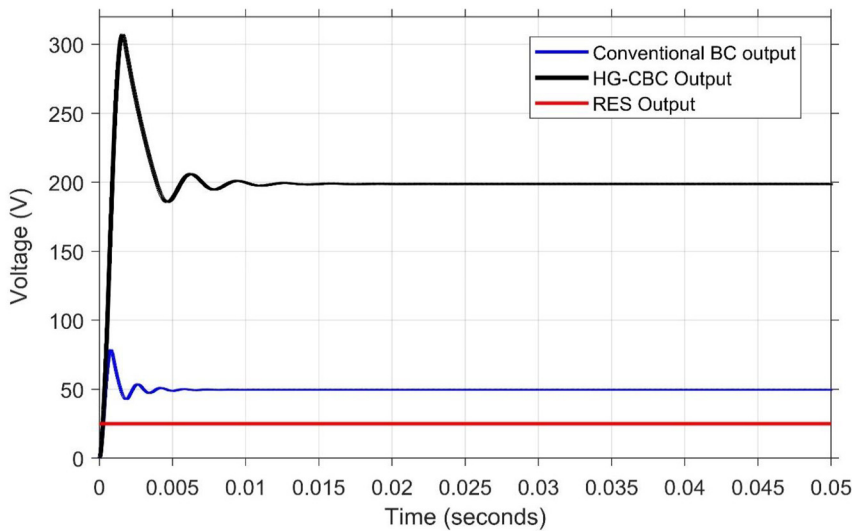
Figure 25: Output voltage of RES and HG-CBC.

output is two times the boost factor, resulting in a V_{out} of 50 V. This voltage is insufficient for grid integration. So, the HG-CBC topology is proposed to improve the output by eight times, resulting in a V_{out} of 200 V.

9 Conclusions

The goal of this research is to afford a unique, extensive, perceptive, and comparative analysis of various HG-BC configurations for RES and EV applications. The operating principle and mathematical modeling of the HG-QFBC, HG-QBC, HG-IBC, HG-IQBC, and HG-CBC topologies have been reviewed, analyzed, and discussed. For a 0.5 duty cycle,

a detailed comparison of various HG-BC is made in terms of B and component count.

Furthermore, for the above-mentioned HG-BC topologies, simulation has been carried out by employing the MATLAB/Simulink tool. The evaluation is done based on theoretical comparisons of performance traits like voltage gain, boost factor, and number of components.

References

Acar, C., and I. Dincer. 2017. "Environmental Impact Assessment of Renewables and Conventional Fuels for Different End Use Purposes." *International Journal of Global Warming* 13 (3–4): 260–77.

Ali, M. S., S. K. Kamarudin, M. S. Masdar, and A. Mohamed. 2014. "An Overview of Power Electronics Applications in Fuel Cell Systems: DC and AC Converters." *The Scientific World Journal* 2014: 1–9.

Aihsan, M. Z., M. M. Azizan, M. I. Fahmi, A. M. Yusof, and M. F. Hariz. 2022. "High Gain DC/DC Boost Converter for Electrical Vehicle Applications." In *Proceedings of the 6th International Conference on Electrical, Control and Computer Engineering*, 69–78. Singapore: Springer.

Ahmad, M., A. Moumin, F. Panhwar, and A. Adam. 2018. *High Gain Non-Isolated DC-DC Converter Topologies for Energy Conversion Systems*. Doctoral dissertation. Board Bazar, Gazipur: Department of Electrical and Electronic Engineering, Islamic University of Technology.

Ahmad, J., I. Pervez, A. Sarwar, M. Tariq, M. Fahad, R. K. Chakrabortty, and M. J. Ryan. 2020. "Performance Analysis and Hardware-In-The-Loop (HIL) Validation of Single Switch High Voltage gain DC–DC Converters for MPP Tracking in Solar PV System." *IEEE Access* 9: 48811–30.

Alghaythi, M. L., R. M. O'Connell, N. E. Islam, M. M. S. Khan, and J. M. Guerrero. 2020. "A High Step-Up Interleaved DC-DC Converter with Voltage Multiplier and Coupled Inductors for Renewable Energy Systems." *IEEE Access* 8: 123165–74.

Chandrasekar, B., C. Nallaperumal, S. Padmanaban, M. S. Bhaskar, J. B. Holm-Nielsen, Z. Leonowicz, and S. O. Masebinu. 2020. "Non-isolated High-Gain Triple Port DC–DC Buck-Boost Converter with Positive Output Voltage for Photovoltaic Applications." *IEEE Access* 8: 113649–66.

Dawood, N. B. 2016. "Review of Different DC to DC Converters Based for Renewable Energy Applications." *International Research Journal of Engineering and Technology* 3 (3): 46–50.

Elsayad, N., H. Moradisizkoohi, and O. Mohammed. 2018. "A New Three-Level Flying-Capacitor Boost Converter with an Integrated LC 2 D Output Network for Fuel-Cell Vehicles: Analysis and Design." *Inventions* 3 (3): 61.

Forouzesh, M., Y. P. Siwakoti, S. A. Gorji, F. Blaabjerg, and B. Lehman. 2017. "Step-up DC–DC Converters: A Comprehensive Review of Voltage-Boosting Techniques, Topologies, and Applications." *IEEE Transactions on Power Electronics* 32 (12): 9143–78.

Gore, S., P. K. Maroti, M. Al-Hitmi, and A. Iqbal. 2019. "A Dual Output High Gain DC-to-DC Converter for Electric Vehicle Application." In *2019 International Conference on Power Electronics, Control and Automation (ICPECA)*, 1–6. New Delhi: IEEE.

Hasanpour, S., Y. P. Siwakoti, and F. Blaabjerg. 2022. "A New High Efficiency High Step-Up DC/DC Converter for Renewable Energy Applications." *IEEE Transactions on Industrial Electronics* 70 (2): 1489–500.

Hossain, M. Z., and N. A. Rahim. 2018. "Recent Progress and Development on Power DC–DC Converter Topology, Control, Design and Applications: A Review." *Renewable and Sustainable Energy Reviews* 81: 205–30.

Hosseini, S. H., R. S. Alishah, and N. V. Kurdkandi. 2015. "Design of a New Extended Zeta Converter with High Voltage Gain for Photovoltaic Applications." In *2015 9th International Conference on Power Electronics and ECCE Asia (ICPE-ECCE Asia)*, 970–7. Seoul: IEEE.

Jagadeesh, I., and V. Indragandhi. 2022. "Comparative Study of DC–DC Converters for Solar PV with Microgrid Applications." *Energies* 15 (20): 7569.

Kabalo, M., B. Blunier, D. Bouquain, and A. Miraoui. 2010. "State-of-the-Art of DC-DC Converters for Fuel Cell Vehicles." In *2010 IEEE Vehicle Power and Propulsion Conference*, 1–6. Lille: IEEE.

Keerthana, R., and N. J. Chintu. 2017. "Performance Analysis of Zeta Converter in Wind Power Application." *Asian Journal of Applied Science and Technology* 1 (3): 199–203.

Khare, V., S. Nema, and P. Baredar. 2013. "Status of Solar Wind Renewable Energy in India." *Renewable and Sustainable Energy Reviews* 27: 1–10.

Kumar, B. M., S. N. Rao, and M. S. Indira. 2022. "Analysis of Grid-Connected Reduced Switch MLI with High-Gain Interleaved Boost Converter and Hybrid MPPT for Solar PV." *International Journal of Energy and Environmental Engineering* 1–21, https://doi.org/10.1007/s40095-022-00479-4.

Manikandan, A., and N. Vadivel. 2013. "Design and Implementation of Luo Converter for Electric Vehicle Applications." *International Journal of Engineering Trends and Technology* 4 (10): 4437–41.

Mansour, A. S., A. H. H. Amer, E. E. El-Kholy, and M. S. Zaky. 2022. "High Gain DC/DC Converter with Continuous Input Current for Renewable Energy Applications." *Scientific Reports* 12 (1): 1–22.

Mansour, A. S., and M. S. Zaky. 2023. "A New Extended Single-Switch High gain DC–DC Boost Converter for Renewable Energy Applications." *Scientific Reports* 13 (1): 264.

Maroti, P. K., S. Padmanaban, J. B. Holm-Nielsen, M. S. Bhaskar, M. Meraj, and A. Iqbal. 2019. "A New Structure of High Voltage Gain SEPIC Converter for Renewable Energy Applications." *IEEE Access* 7: 89857–68.

Matam, M. B., A. K. D. Venkata, and V. K. Mallapu. 2018. "Analysis and Implementation of Impedance Source Based Switched Capacitor Multi-Level Inverter." *Engineering Science and Technology, An International Journal* 21 (5): 869–85.

Meinagh, F. A. A., V. Ranjbarizad, and E. Babaei. 2019. "New Non-Isolated High Voltage gain Single-Switch DC-DC Converter Based on Voltage-Lift Technique." In *2019 10th International Power Electronics, Drive Systems and Technologies Conference (PEDSTC)*, 219–23. Shiraz: IEEE.

Moradpour, R., H. Ardi, and A. Tavakoli. 2017. "Design and Implementation of a New SEPIC-Based High Step-Up DC/DC Converter for Renewable Energy Applications." *IEEE Transactions on Industrial Electronics* 65 (2): 1290–7.

Mumtaz, F., N. Z. Yahaya, S. T. Meraj, B. Singh, R. Kannan, and O. Ibrahim. 2021. "Review on Non-isolated DC–DC Converters and Their Control Techniques for Renewable Energy Applications." *Ain Shams Engineering Journal* 12 (4): 3747–63.

Nagaraja Rao, S., S. K. Anisetty, B. M. Manjunatha, B. M. Kiran Kumar, V. Praveen Kumar, and S. Pranupa. 2022. "Interleaved High-Gain Boost Converter Powered by Solar Energy Using Hybrid-Based Mpp Tracking Technique." *Clean Energy* 6 (3): 460–75.

Naresh, S. V. K., S. Peddapati, and M. L. Alghaythi. 2021. "Non-Isolated High Gain Quadratic Boost Converter Based on Inductor's Asymmetric Input Voltage." *IEEE Access* 9: 162108–21.

Navamani, J. D., A. Lavanya, D. Almakhles, and M. J. Sathik. 2022. "A Review on Segregation of Various High Gain Converter Configurations for Distributed Energy Sources." *Alexandria Engineering Journal* 61 (1): 675–700.

Perera, F. 2018. "Pollution from Fossil-Fuel Combustion is the Leading Environmental Threat to Global Pediatric Health and Equity: Solutions Exist." *International Journal of Environmental Research and Public Health* 15 (1): 16.

Pranupa, S., A. T. Sriram, and S. Nagaraja Rao. 2022. "Wind energy conversion system using perturb & observe-based maximum power

point approach interfaced with T-type three-level inverter connected to grid." *Clean Energy* 6 (4): 534–49.

Purushothaman, S. K., D. Sattianadan, and K. Vijayakumar. 2022. "Novel Compact Design High gain DC–DC Step Up Converter Applicable for PV Applications." *Sustainable Energy Technologies and Assessments* 51: 101720.

Radhika, S., and V. Margaret. 2021. "A Review on DC-DC Converters with Photovoltaic System in DC Micro Grid." In *Journal of Physics: Conference Series*, Vol. 1804, 1st ed., 012155. IOP Publishing.

Raghavendra, K. V. G., K. Zeb, A. Muthusamy, T. N. V. Krishna, S. V. P. Kumar, D. H. Kim, M. S. Kim, H. G. Cho, and H. J. Kim. 2019. "A Comprehensive Review of DC–DC Converter Topologies and Modulation Strategies with Recent Advances in Solar Photovoltaic Systems." *Electronics* 9 (1): 31.

Rahimi, T., L. Ding, H. Gholizadeh, R. S. Shahrivar, and R. Faraji. 2021. "An Ultra High Step-Up DC–DC Converter Based on the Boost, Luo, and Voltage Doubler Structure: Mathematical Expression, Simulation, and Experimental." *IEEE Access* 9: 132011–24.

Rao, S. N., Veerabhadra, and P. Kumar. 2020. "Performance Analysis of Z-Source Inverter Topologies for Renewable Energy Sources and Fuel Cell Applications." In *2020 IEEE International Conference on Distributed Computing, VLSI, Electrical Circuits and Robotics (DISCOVER)*, 165–70. Udupi: IEEE.

Raveendhra, D., P. Rajana, K. S. R. Kumar, P. Jugge, R. Devarapalli, E. Rusu, and H. H. Fayek. 2022. "A High-Gain Multiphase Interleaved Differential Capacitor Clamped Boost Converter." *Electronics* 11 (2): 264.

Reddy, D. S. 2021. "Review on Power Electronic Boost Converters." *Australian Journal of Electrical and Electronics Engineering* 18 (3): 127–37.

Rehman, Z., I. Al-Bahadly, and S. Mukhopadhyay. 2015. "Multiinput DC–DC Converters in Renewable Energy Applications–An Overview." *Renewable and Sustainable Energy Reviews* 41: 521–39.

Revathi, B. S., and M. Prabhakar. 2016. "Non Isolated High gain DC–DC Converter Topologies for PV Applications–A Comprehensive Review." *Renewable and Sustainable Energy Reviews* 66: 920–33.

Sabzali, A. J., E. H. Ismail, and H. M. Behbehani. 2015. "High Voltage Step-Up Integrated Double Boost–Sepic DC–DC Converter for Fuel-Cell and Photovoltaic Applications." *Renewable Energy* 82: 44–53.

Samuel, V. J., G. Keerthi, and P. Mahalingam. 2020. "Non-Isolated DC–DC Converter with Cubic Voltage gain and Ripple-Free Input Current." *IET Power Electronics* 13 (16): 3675–85.

Shahir, F. M., E. Babaei, and M. Farsadi. 2017. "Voltage-Lift Technique Based Non-Isolated Boost DC–DC Converter: Analysis and Design." *IEEE Transactions on Power Electronics* 33: 5917–26.

Sivakumar, S., M. J. Sathik, P. S. Manoj, and G. Sundararajan. 2016. "An Assessment on Performance of DC–DC Converters for Renewable Energy Applications." *Renewable and Sustainable Energy Reviews* 58: 1475–85.

Suryoatmojo, H., R. Mardiyanto, D. C. Riawan, S. Anam, E. Setijadi, S. Ito, and I. Wan. 2018. "Implementation of High Voltage Gain DC–DC Boost Converter for Fuel Cell Application." In *2018 International Conference on Engineering, Applied Sciences, and Technology (ICEAST)*, 1–4. Phuket: IEEE.

Torkan, A., and M. Ehsani. 2018. "A Novel Nonisolated Z-Source DC–DC Converter for Photovoltaic Applications." *IEEE Transactions on Industry Applications* 54 (5): 4574–83.

Varanasi, P. K., S. Nagaraja Rao, and P. Duraiswamy. 2023. "Intelligent Control of Double Boost Converter Interfaced with Multilevel Inverter for Electrical Vehicle Applications." *Journal of The Institution of Engineers (India): Series B*, https://doi.org/10.1007/s40031-022-00828-1.

Veerabhadra, and S. Nagaraja Rao. 2022. "Assessment of High-Gain Quadratic Boost Converter with Hybrid-Based Maximum Power Point Tracking Technique for Solar Photovoltaic Systems." *Clean Energy* 6 (4): 632–45.

Veerachary, M., and N. Kumar. 2020. "Analysis and Design of Quadratic Following Boost Converter." *IEEE Transactions on Industry Applications* 56 (6): 6657–73.

Wu, B., S. Li, Y. Liu, and K. M. Smedley. 2015. "A New Hybrid Boosting Converter for Renewable Energy Applications." *IEEE Transactions on Power Electronics* 31 (2): 1203–15.

Zaid, M., C. H. Lin, S. Khan, J. Ahmad, M. Tariq, A. Mahmood, A. Sarwar, B. Alamri, and A. Alahmadi. 2021. "A Family of Transformerless Quadratic Boost High Gain DC–DC Converters." *Energies* 14 (14): 4372.

Zaid, M., I. H. Malick, I. Ashraf, M. Tariq, B. Alamri, and E. M. Rodrigues. 2022. "A Nonisolated Transformerless High-Gain DC–DC Converter for Renewable Energy Applications." *Electronics* 11 (13): 2014.

Zhang, N., D. Sutanto, and K. M. Muttaqi. 2016. "A Review of Topologies of Three-Port DC–DC Converters for the Integration of Renewable Energy and Energy Storage System." *Renewable and Sustainable Energy Reviews* 56: 388–401.